Robust Predictive Torque Control of N*3-phase PMSM for High Power Traction Application

Wu, Gongping; Huang, Sheng; Wu, Qiuwei; Rong, Fei; Zhang, Changfan; Liao, Wu

Published in:
IEEE Transactions on Power Electronics

Link to article, DOI:
10.1109/tpel.2020.2981914

Publication date:
2020

Document Version
Peer reviewed version

Robust Predictive Torque Control of *N**3-phase PMSM for High Power Traction Application

Gongping Wu, Sheng Huang, Qiuwei Wu, *Senior Member IEEE,*

Fei Rong, *Member IEEE*, Changfan Zhang, Wu Liao

Abstract—The permanent magnet synchronous motor (PMSM) has become a core component of electromechanical energy conversion in the modern industrial field. In order to expand the application of the PMSM in the field of high power traction, a robust predictive torque control (R-PTC) strategy for the *N*-segment three-phase PMSM (*N3-phase PMSM) is proposed in this paper. Firstly, the output characteristics of the *N**3-phase PMSM are illustrated with the finite element analysis method, and the mathematical model is established. Then, the six-segment three-phase PMSM predictive control system driven by six parallel inverters is designed to generate the required torque. Further, the influence of the parameter mismatch on the predicted torque and stator flux is taken into consideration based on the conventional predictive torque control (PTC). Finally, a novel R-PTC method with the proportional controller is developed for the *N**3-phase PMSM, which can effectively improve accuracy and robustness of predictive control performance under parameters mismatch. Simulation and experimental results verify that, compared with the conventional PTC, the proposed R-PTC method can make the predicted stator flux and torque value accurately track its reference values while achieving lower stator flux and torque ripple.**

Index Terms — *N*-segment three-phase PMSM, multi-phase, predictive torque control, high power traction, parameters mismatch.

Manuscript received October 18, 2019; revised January 23, 2020; accepted March 15, 2020. This work was supported in part by the National Key Research and Development Program of China under Grant 2018YFB0606000, in part by Hunan Provincial Innovation Key Foundation for Postgraduate under Grant CX20190261 and in part by the China Scholarship Council (CSC) under Grant 201906130062. (*Corresponding author: Sheng Huang*.)

G. Wu is with the College of Electrical and Information Engineering, Hunan University, Changsha, 410082, China and Center for Electric and Energy (CEE), Department of Electrical Engineering, Technical University of Denmark (DTU), Kgs. Lyngby 2800, Denmark (e-mail: gongping_wu@hnu.edu.cn).

S. Huang and Q. Wu are with the Center for Electric and Energy (CEE), Department of Electrical Engineering, Technical University of Denmark (DTU), Kgs. Lyngby 2800, Denmark (e-mail: huang98123@163.com, qw@elektro.dtu.dk).

C. Zhang is with the College of Electrical and Information Engineering, Hunan University of Technology, Zhuzhou 412000, China (e-mail: zcf@hut.edu.cn).

F. Rong and W. Liao are with the College of Electrical and Information Engineering, Hunan University, Changsha, 410082, China(e-mail: rf_hunu@126.com, liaowu1988@hnu.edu.cn).

I. Introduction

PERMANENT magnet synchronous motors (PMSMs) have become the key and core components of complex electromechanical systems, such as urban rail vehicles, ship propulsion, high-speed elevators, and wind power generation, due to its advantages of fast dynamic torque response, high overload capability and wide speed range [1-4]. Although three-phase PMSMs are quite common in various industrial fields, multi-phase PMSMs have unique advantages in special applications requiring of redundancy and high power [5,6]. Compared with traditional three-phase PMSMs, the multi-phase PMSMs can provide higher torque and power density under the same voltage vector [7,8], especially suitable for high power traction applications. With the improvement of power level, the multi-phase PMSMs has become inevitable in the field of high power traction [9]. Compared with the conventional multi-phase PMSM, the proposed *N**3-phase PMSM structure has extremely higher torque quality and lower cogging. Furthermore, the control strategy of *N**3-phase PMSM is more simple because it can be driven by several independent three-phase voltage source inverter [9-11].

The efficient control strategy is an essential part of multi three-phase PMSM drives. The improvement of control strategy can greatly enhance the performance of the drive system and the whole application. In recent years, some methods have been investigated to control multi three-phase PMSM more effectively. In [9, 12, 13], a novel multi three-phase PMSM was proposed for high power traction applications. Compared with the conventional multi-phase PMSM, the control algorithm is easy to implement, which is similar to the traditional three-phase PMSM control algorithm. In [14,15], a two-segment three-phase PMSM system powered by two inverters with phase-shift PWM has been developed, which can fulfill the requirement of high power and mitigation of torque ripple. In [16,17], a dual three level T-type neutral-point clamped inverter fed dual PMSM topology was proposed for the high power automotive applications, which can reduce current stress and capacitors' voltage deviation. In [12-17], the PI controller was adopted to control the multi three-phase PMSM, which can obtain the perfect steady state control performance. However, in practice, the multi three-phase PMSM is a time-varying control system with parameter variations, as well as uncertain disturbances. It is difficult for PI controller to obtain a satisfying dynamic control performance in the whole operating range of the time-varying system [18].

The quick dynamic response and torque smoothness are the important criterion that decides the performance of the multi three-phase PMSM system. Compared with classical PI control, the predictive torque control (PTC) has attracted extensive attention in the PMSM control due to its excellent dynamic and steady-state performance and less torque ripple [20-28]. The stator flux and torque error-based cost function is usually utilized in the PTC method, which can accurately predict the behavior of stator flux and torque. Thus, the weighting factor of cost function is the critical factor to determine the control performance between stator flux and torque. However, it is a very complex task to obtain the suitable weighting factor over the entire operating range of the motor [19]. In [20], a novel predictive stator flux and torque control techniques without weighting factor was developed, which can avoid the tuning of weighting factor calculation for a correct operation. In [21], an improved finite control set-model predictive control with an imposed optimized weighting factor was proposed, which can obtain less torque ripple in wide speed range. In [22, 23], a predictive control strategy using a discrete-time state space model was presented for PMSM, which can eliminate the requirement of weighting factors in the PTC method. Although these methods have been proved to be very effective in eliminating weighting factors of cost function, the influence of the parameter mismatch on the predicted torque and stator flux is not considered [20-23].

The parameters utilized in the predictive controller are not able to remain actual *N**3-phase PMSM parameters values all the time due to the identification errors or the high temperature operation [24]. Model parameters mismatch deteriorates the control performance of PTC method and results in torque ripple increases if the parameter mismatch is not considered in modified controller design. The design of disturbance observer is the main approach to eliminate the parameters mismatch. In [25-27], a robust fault-tolerant predictive control strategy based on a composite discrete observer was developed for PMSMs, which can reduce the impact of motor parameter perturbation. In [28], a flux immunity robust predictive control with incremental model and extended state observer was presented for PMSM Drive, which can improve robustness against inductance mismatch and overcome rotor flux effects. In [29], a robust sensor less PTC method with the full order and reduced order observers was proposed, which can improve the robustness of the uncertain stator and rotor resistances. In [30], a novel encoder less finite control set PTC method with a robust adaptive observer was developed, which can achieve the strong robustness of the uncertain stator flux and rotor flux parameters. In [31], a disturbance observer-based PTC approach was investigated, which can improve the system disturbance rejection ability against the parameter uncertainties and time delays. Although the methods in [25-31] can achieve perfect control performance under parameters mismatch, the PTC method based on disturbance observer compensation relies heavily on the accurate measurement of voltage and current.

Instead of adopting observer compensation, a modified PTC method with weighting factor was proposed in [32], which can reduce the torque ripple at the presence of parametric uncertainty by improving the prediction accurateness. In [33], an extension of the PTC method was proposed by using two-degree-of-freedom control, which can make PMSM drive system more robust in the presence of parameter mismatch. However, only the case of inductance parameter mismatch was considered in [32, 33], and the flux linkage parameter mismatch will also seriously affect the performance of the PTC method. In this paper, a R-PTC techniques for the *N**3-phase PMSM is proposed to enhance robustness against parameters mismatch and operate without the weighting factor of cost function. The proportional controller is used to replace the disturbance observer compensation in this paper to eliminate the influence of the inductance parameter mismatch and flux linkage parameter mismatch. Compare with the conventional PTC method, the R-PTC techniques with proportional controller can effectively eliminate the steady errors of the stator flux and obtain the lower torque ripple. Simulation and experimental results both validate the excellent performance of the R-PTC techniques.

This paper is organized as follows. The mathematical model and drive system structure of *N**3-phase PMSM is presented in section II. The parameter sensitivity analysis of conventional PTC method is analyzed in Section III. The R-PTC method of *N**3-phase PMSM with parameters mismatch is proposed in Section IV. The simulations and experiments are setup in Section V and Section VI, respectively. Section VII concludes this paper.

II. Mathematical Model and Drive System Structure of *N**3-phase PMSM

Using the concept of unit motor, an *N**3-phase PMSM is developed. The proposed *N**3-phase PMSM consists of *N* motor units with repetitive characteristics. The stator core of *N**3-phase PMSM is composed of unit motor stator punches, and each unit motor is independently connected. Therefore, the *N**3-phase PMSM can be modularized and assembled with simple structure, and each unit motor has the isolation characteristics of electrical, magnetic and thermal. Taking *6**3-phase PMSM as an example, the structure diagram of *6**3-phase PMSM is shown in Fig. 1. The stator winding arrangement is an important part of the *N**3-phase PMSM. The stator winding arrangement of the unit motor can be similar to that of the traditional three-phase PMSM. The star of slots for the *6**3-phase PMSM is shown in Fig. 2, with each phase sharing six identical slot vectors.

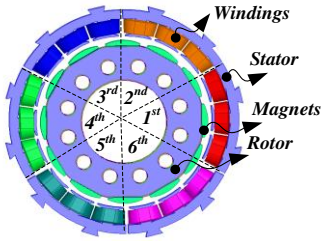

*Fig. 1. Structure diagram of 6*3- phase PMSM.*

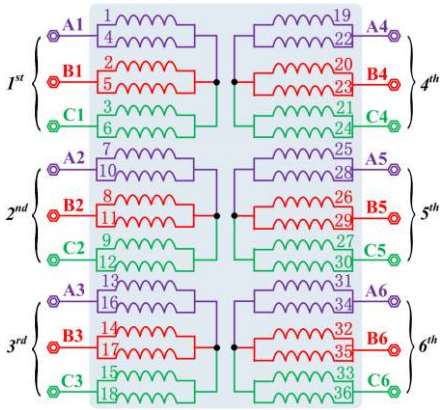

*Fig. 2. Stator winding connection of 6*3- phase PMSM.*

*A. Mathematical Model of N*3-phase PMSM*

According to the characteristics analysis of the *N**3-phase PMSM, the mathematical model of the *N**3-phase PMSM can be equivalent to that of the traditional three-phase PMSM. According to [9, 13], the voltage state-space equations of the *N**3-phase PMSM can be expressed as the traditional voltage equations of the PMSM. Thus, the d- and q-axis voltage transformation of one winding set can be described as follows:

$$\begin{cases} \begin{bmatrix} u_{dj} \\ u_{qj} \end{bmatrix} = \frac{2}{3} \begin{bmatrix} \cos\theta & \cos(\theta - \frac{2\pi}{3}) & \cos(\theta + \frac{2\pi}{3}) \\ \sin\theta & \sin(\theta - \frac{2\pi}{3}) & \sin(\theta + \frac{2\pi}{3}) \end{bmatrix} \begin{bmatrix} u_{aj} \\ u_{bj} \\ u_{cj} \end{bmatrix} \\ j=1,2,3,\cdots N \end{cases} \quad (1)$$

where j stands for any unit of the motor, u_{dj} and u_{qj} represent the *d*-and *q*-axis voltages of the *j* th winding, respectively ; u_{aj}, u_{bj} and u_{cj} represent the *a, b*-and *c*-axis voltages of the *j* th winding, respectively; θ is the rotor position angle.

The *N**3-phase PMSM is composed of three-phase PMSM units with identical characteristics. Therefore, the stator resistance and stator inductance of each three-phase PMSM unit are equal. The *d*-and *q*-axis voltage equations of *N**3-phase surface-mounted PMSM (*N**3-phase SPMSM) unit are as follows [12-14]:

$$\begin{cases} \frac{di_{dj}}{dt} = -\frac{R_o}{L_o} i_{dj} + \omega_e i_{qj} + \frac{1}{L_o} u_{dj} \\ \frac{di_{qj}}{dt} = -\frac{R_o}{L_o} i_{qj} - \omega_e i_{dj} - \frac{\psi_{ro}}{L_o} \omega_e + \frac{1}{L_o} u_{qj} \end{cases} \quad (2)$$

where i_{dj} and i_{qj} are the d-and q-axis currents, respectively; R_o and L_o are the stator resistance and stator inductance, respectively; ω_e is the electrical rotor speed, ψ_{ro} is the flux linkage of permanent magnets.

According to the characteristics of *N**3-phase PMSM, it is known that the output electromagnetic torque of *N**3-phase SPMSM is the sum of the electromagnetic torque produced by each three-phase SPMSM unit. The electromagnetic torque produced by the *N**3-phase SPMSM is as follows [12, 13]:

$$T_e = \frac{3n_p}{2} \sum_{j=1}^{N} (\psi_{ro} i_{qj}) = \frac{3Nn_p}{2} \psi_{ro} i_{qj} \quad (3)$$

The mechanical dynamic model of *N**3-phase SPMSM can be described as follows:

$$T_e - T_L = \frac{J}{n_p} \frac{d\omega_e}{dt} \quad (4)$$

where n_p is the number of pole pairs; J is the moment of inertia; T_e and T_L are the electromagnetic torque and load torque of the *N**3-phase SPMSM, respectively.

*B. Drive system structure of N*3-phase PMSM*

Taking *6**3-phase PMSM as an example, the *6**3-phase PMSM is driven by six drive units to obtain required torque. The six-segment stator winding of *6**3-phase PMSM are respectively connected with six voltage source inverters (VSIs) in parallel, as shown in Fig. 3. Each group of stator windings is excited independently with three-phase symmetrical voltage generated by a VSI. The VSIs of *6**3-phase PMSM are electrically separated from each other. According to the characteristics of *N**3-phase PMSM, the mathematical model and characteristic of each motor units is identical with a regular PMSM, and all the characteristics of each motor units are repetitive. In addition, the voltage-seconds characteristic of any two VSIs should be the same [14-16]. The control of a VSI can be analogous to that of a conventional inverter [12, 34].

In order to make the control algorithm simple and easy to implement, this paper uses a set of the PTC algorithm to send out six groups of the same modulation signals at the same time, as shown in Fig. 3. The six groups of the same modulation signals are input into six parallel inverters, respectively.

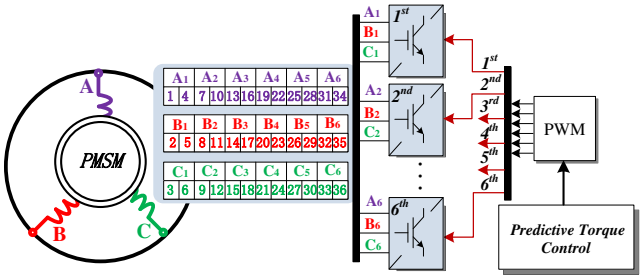

*Fig. 3. Drive system structure diagram of 6*3-phase PMSM.*

III. Parameter Sensitivity Analysis of Conventional PTC

The purpose of PTC strategy is to control the torque and stator flux of motor. The structural diagram of the conventional PTC method is illustrated, as shown in Fig. 4.

In order to minimize the absolute error between the predicted stator flux and torque values with its reference values, the cost function can be defined as follows [32]:

$$g = k_\psi \left| \psi_s^{ref} - \psi_s(k+1) \right| + \left| T_e^{ref} - T_e(k+1) \right| \quad (5)$$

where k_ψ is a weighting factor; T_e^{ref} and ψ_s^{ref} are the torque reference value and flux linkage reference value, respectively; $T_e(k+1)$ and $\psi_s(k+1)$ are the predicted torque value and predicted flux linkage value, respectively.

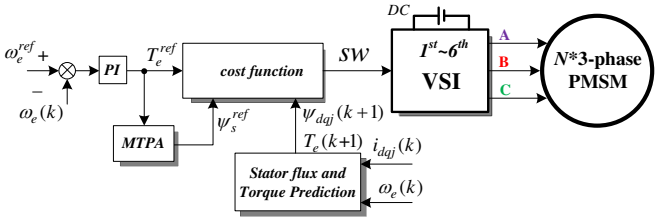

Fig. 4. Structural diagram of the conventional PTC method.

If the PTC sampling period T_s is short enough, the discrete form of *N**3-phase SPMSM can be modeled by the first-order Taylor expansion. According to (2) and (3), the torque and stator flux prediction equation of *N**3-phase SPMSM can be expressed as

$$\begin{cases} \psi_s(k+1)=\sqrt{\psi_{dj}^2(k+1)+\psi_{qj}^2(k+1)} \\ T_e(k+1)=\dfrac{3n_p}{2}\sum_{j=1}^{N}(\psi_{ro}i_{qj}(k+1)) \end{cases} \tag{6}$$

The discrete form of Eq. (2) can be obtained as

$$\begin{cases} i_{qj}(k+1)=i_{qj}(k)+\dfrac{T_s}{L_o}\left[-L_o\omega(k)i_{dj}(k)-R_oi_{qj}(k)-\omega(k)\psi_{ro}+u_{qj}(k)\right] \\ \psi_{dj}(k+1)=u_{dj}(k)T_s+(1-\dfrac{R_o}{L_o}T_s)\psi_{dj}(k)+\omega_e(k)T_s\psi_{qj}(k)+\dfrac{R_o}{L_o}\psi_{ro}T_s \\ \psi_{qj}(k+1)=u_{qj}(k)T_s-\omega_e(k)T_s\psi_{dj}(k)+(1-\dfrac{R_o}{L_o}T_s)\psi_{qj}(k) \end{cases} \tag{7}$$

where $\psi_{dj}(k)$ and $\psi_{qj}(k)$ are the d-and q-axis stator flux components, respectively.

The PTC strategy is a discrete control algorithm based on the precise mathematical model of *N**3-phase SPMSM. From (7), it can be found that the torque and stator flux prediction equation are absolutely dependent on the motor parameters (i.e., ψ_{ro}, R_o and L_o), which means that these parameters mismatch would result in inaccurate prediction of *N**3-phase SPMSM drive system. Furthermore, the motor parameters mismatch leads to increasing torque and flux ripples and deteriorates the performance of the PTC algorithm.

In order to evaluate the sensitivity of the PTC algorithm response to a parameter, let us analyze the torque prediction model according to (7). Introducing $R=R_o+\Delta R$, $L=L_o+\Delta L$ and $\psi_r=\psi_{ro}+\Delta\psi_r$, where R_o, L_o, and ψ_{ro} are actual values and ΔR, ΔL, and $\Delta\psi_r$ are uncertain components of the corresponding parameter. The (7) is rewritten as follows when parameters mismatch are considered.

$$\begin{cases} i_{qj}(k+1)=i_{qj}(k)-\omega(k)i_{dj}(k)T_s-\dfrac{R_o+\Delta R}{L_o+\Delta L}i_{qj}(k)T_s \\ \qquad -\dfrac{\psi_{ro}+\Delta\psi_r}{L_o+\Delta L}\omega(k)T_s+\dfrac{1}{L_o+\Delta L}u_{qj}(k)T_s \\ \psi_{dj}(k+1)=u_{dj}(k)T_s+\psi_{ro}+\Delta\psi_r+(L_o+\Delta L)[i_{dj}(k)+i_{qj}(k)\omega_e(k)T_s] \\ \qquad -\dfrac{R_o+\Delta R}{L_o+\Delta L}T_s\left[\Delta\psi_r+(L_o+\Delta L)i_{dj}(k)\right] \\ \psi_{qj}(k+1)=u_{qj}(k)T_s-\omega_e(k)T_s\left[\psi_{ro}+\Delta\psi_r+(L_o+\Delta L)i_{dj}(k)\right] \\ \qquad +(1-\dfrac{R_o+\Delta R}{L_o+\Delta L}T_s)(L_o+\Delta L)i_{qj}(k) \end{cases} \tag{8}$$

It should be noted that the value of stator resistance voltage is much smaller than the amplitude of the voltage source when the motor operates stably (e.g., $\left|\frac{R_o+\Delta R}{L_o+\Delta L}i_{dj,qj}(k)\right| << \left|\frac{1}{L_o+\Delta L}u_{dj,qj}(k)\right|$). Thus, the term $\left|\frac{R_o+\Delta R}{L_o+\Delta L}i_{dj,qj}(k)\right|$ does not have any negative effect on torque and stator flux prediction. It can be inferred that the stator resistance parameter mismatch does not have any considerable effect on torque prediction as well as stator flux linkage prediction. However, the inductance parameter mismatch and flux linkage parameter mismatch will lead to non-optimal switching state and increase the prediction bias. Torque and stator flux ripple of the *N**3-phase PMSM drive system will also increase if the model parameters mismatch are not considered in the design of the robust predictive controller.

IV. R-PTC Method of *N**3-phase PMSM with Parameters Mismatch

According to (2), the d-and q-axis voltage equations of *N**3-phase SPMSM under inductance parameter mismatch and flux linkage parameter mismatch can be expressed as follows:

$$\begin{cases} \dfrac{di_{dj}}{dt}=-\dfrac{R_o}{L_o}i_{dj}+\omega_e i_{qj}+\dfrac{1}{L_o}u_{dj}-\dfrac{1}{L_o}f_{dj} \\ \dfrac{di_{qj}}{dt}=-\omega_e i_{dj}-\dfrac{R_o}{L_o}i_{qj}-\dfrac{\psi_{ro}}{L_o}\omega_e+\dfrac{1}{L_o}u_{qj}-\dfrac{1}{L_o}f_{qj} \end{cases} \tag{9}$$

with

$$\begin{aligned} f_{dj}&=\frac{\Delta L}{(L_o+\Delta L)}(u_{dj}-R_oi_{dj}+L_o\omega_e i_{qj}+\Delta L\omega_e i_{qj})-\Delta L\omega_e i_{qj} \\ f_{qj}&=\frac{\Delta L}{(L_o+\Delta L)}(u_{qj}-R_oi_{qj}-L_o\omega_e i_{dj}-\Delta L\omega_e i_{dj}-\omega_e\psi_{ro}-\omega_e\Delta\psi_r) \\ &\quad +\Delta L\omega_e i_{dj}+\omega_e\Delta\psi_r \end{aligned} \tag{10}$$

where f_{dj} and f_{qj} are the d-and q-axis uncertain disturbances caused by inductance parameter mismatch and flux linkage parameter mismatch, respectively.

From (9), the d-and q-axis flux linkage equations of *N**3-phase SPMSM can be obtained as follows:

$$\begin{cases}\begin{bmatrix}\dfrac{d\psi_{dj}}{dt}\\ \dfrac{d\psi_{qj}}{dt}\end{bmatrix}=\begin{bmatrix}u_{dj}\\ u_{qj}\end{bmatrix}+\begin{bmatrix}-\dfrac{R_o}{L_o} & \omega_e\\ -\omega_e & -\dfrac{R_o}{L_o}\end{bmatrix}\begin{bmatrix}\psi_{dj}\\ \psi_{qj}\end{bmatrix}+\begin{bmatrix}\dfrac{R_o}{L_o}\psi_{ro}\\ 0\end{bmatrix}-\begin{bmatrix}f_{dj}\\ f_{qj}\end{bmatrix}\\ \begin{bmatrix}\psi_{dj}\\ \psi_{qj}\end{bmatrix}=\begin{bmatrix}L_o & 0\\ 0 & L_o\end{bmatrix}\begin{bmatrix}i_{dj}\\ i_{qj}\end{bmatrix}+\begin{bmatrix}\psi_{ro}\\ 0\end{bmatrix}\end{cases} \tag{11}$$

The discrete expression of (11) is

$$\begin{bmatrix}\psi_{dj}(k+1)\\ \psi_{qj}(k+1)\end{bmatrix}=\begin{bmatrix}u_{dj}(k)T_s\\ u_{qj}(k)T_s\end{bmatrix}+\begin{bmatrix}1-\dfrac{R_o}{L_o}T_s & \omega_e(k)T_s\\ -\omega_e(k)T_s & 1-\dfrac{R_o}{L_o}T_s\end{bmatrix}\begin{bmatrix}\psi_{dj}(k)\\ \psi_{qj}(k)\end{bmatrix}+\begin{bmatrix}\dfrac{R_o}{L_o}\psi_{ro}T_s\\ 0\end{bmatrix}-\begin{bmatrix}T_s & 0\\ 0 & T_s\end{bmatrix}\begin{bmatrix}f_{dj}(k)\\ f_{qj}(k)\end{bmatrix} \tag{12}$$

In feedback control system, the most effective means of eliminating static error is to add error feedback adjustment, so we consider adding predictive error feedback in flux linkage equations, (12) is modified to

$$\begin{bmatrix}\psi_{dj}(k+1)\\ \psi_{qj}(k+1)\end{bmatrix}=\begin{bmatrix}u_{dj}(k)T_s\\ u_{qj}(k)T_s\end{bmatrix}+\begin{bmatrix}1-\dfrac{R_o}{L_o}T_s & \omega_e(k)T_s\\ -\omega_e(k)T_s & 1-\dfrac{R_o}{L_o}T_s\end{bmatrix}\begin{bmatrix}\psi_{dj}(k)\\ \psi_{qj}(k)\end{bmatrix}+\begin{bmatrix}\dfrac{R_o}{L_o}\psi_{ro}T_s\\ 0\end{bmatrix}-\begin{bmatrix}Q_1 & 0\\ 0 & Q_2\end{bmatrix}\begin{bmatrix}\Delta\psi_{dj}(k)\\ \Delta\psi_{qj}(k)\end{bmatrix} \tag{13}$$

In order to eliminate the influence of parameters mismatch, the torque prediction equation is modified to

$$T_e(k)=\frac{3Nn_p}{2}\psi_{ro}\frac{\psi_{qj}(k)}{L_o}+Q_3\Delta T_e(k) \tag{14}$$

where $\Delta T_e(k)$ is the torque prediction error between the predicted value and reference value; $\Delta\psi_{dj}(k)$ and $\Delta\psi_{qj}(k)$ are the d-and q-axis flux linkage error between the predicted value and reference value, respectively; Q_1 , Q_2 and Q_3 are the proportional controller parameter.

In steady state, the torque prediction error caused by parameter mismatch can be considered as a constant during one sampling period (i.e., $\Delta T_e(k+1)=\Delta T_e(k)$). According to (14), we can get

$$T_e(k+1)-T_e(k)=\frac{3Nn_p}{2}\psi_{ro}[\frac{\psi_{qj}(k+1)}{L_o}-\frac{\psi_{qj}(k)}{L_o}] \tag{15}$$

Substituting (13) into (15), the relationship between torque and q-axis voltage can be obtained as

$$u_{qj}(k)T_s=G(k) \tag{16}$$

where

$$G(k)=\frac{2L_o}{3Nn_p\psi_{ro}}[T_e(k+1)-T_e(k)]+\omega_e(k)T_s\psi_{dj}(k)+\frac{R_o}{L_o}T_s\psi_{qj}(k)+Q_2\Delta\psi_{qj}(k)$$

.

The influence of resistance voltage can be neglected, therefore, $\frac{R_o}{L_o}T_s\approx 0$ .From (13), the relationship between stator flux amplitude and voltage can be expressed as

$$\begin{aligned}[\psi_s(k+1)]^2&=[\psi_{dj}(k+1)]^2+[\psi_{qj}(k+1)]^2\\ &=[u_{dj}(k)T_s+\psi_{dj}(k)+\omega_e(k)T_s\psi_{qj}(k)-Q_1\Delta\psi_{dj}(k)]^2\\ &\quad+[u_{qj}(k)T_s+\psi_{qj}(k)-\omega_e(k)T_s\psi_{dj}(k)-Q_2\Delta\psi_{qj}(k)]^2\end{aligned} \tag{17}$$

From (17), we can get

$$u_{dj}(k)T_s=\sqrt{[\psi_s(k+1)]^2-F_1(k)}-F_2(k) \tag{18}$$

where $F_1(k)=[G(k)+\psi_{qj}(k)-\omega_e(k)T_s\psi_{dj}(k)-Q_2\Delta\psi_{qj}(k)]^2$, $F_2(k)=[\psi_{dj}(k)+\omega_e(k)T_s\psi_{qj}(k)-Q_1\Delta\psi_{dj}(k)]$.

These values for ψ_s^{ref} and T_e^{ref} are used as the reference in (16) and (18) by considering $\psi_s(k+1)=\psi_s^{ref}$ and $T_e(k+1)=T_e^{ref}$. Thus, the d-and q-axis voltage equations are modified to

$$\begin{cases}u_{dj}(k)=\dfrac{\sqrt{[\psi_s^{ref}]^2-F_1(k)}-F_2(k)}{T_s}\\ u_{qj}(k)=\dfrac{G(k)}{T_s}\end{cases} \tag{19}$$

with

$$\begin{cases}G(k)=\dfrac{2L_o}{3Nn_p\psi_{ro}}[T_e^{ref}-T_e(k)]+\omega_e(k)T_s\psi_{dj}(k)\\ \qquad\quad+\dfrac{R_o}{L_o}T_s\psi_{qj}(k)+Q_2\Delta\psi_{qj}(k)\\ F_1(k)=[G(k)+\psi_{qj}(k)-\omega_e(k)T_s\psi_{dj}(k)-Q_2\Delta\psi_{qj}(k)]^2\\ F_2(k)=[\psi_{dj}(k)+\omega_e(k)T_s\psi_{qj}(k)-Q_1\Delta\psi_{dj}(k)]\end{cases} \tag{20}$$

According to the maximum torque per ample (MTPA), the relationship between stator flux reference and torque reference can be obtained as follows [22]:

$$\psi_s^{ref}=\sqrt{\psi_{dj}^2+\psi_{qj}^2}=\sqrt{\psi_{ro}^2+(L_o\cdot\frac{T_e^{ref}}{\frac{3Nn_p}{2}\psi_{ro}})^2} \tag{21}$$

The structural diagram of the *6*3-phase PMSM drive system with R-PTC strategy is shown in Fig. 5. The proposed R-PTC strategy is used to substitute conventional PTC to enhance robustness against parameters mismatch and eliminate the weighting factor of cost function. The predicted value can accurately track the reference value when there is no parameter mismatch in predictive controller (i.e., Q_1=Q_2=Q_3=0). When parameter mismatch occurs in predictive controller, the errors

between predicted value and reference value can be eliminated by adjusting proportional parameters (i.e., Q_1, Q_2, Q_3).

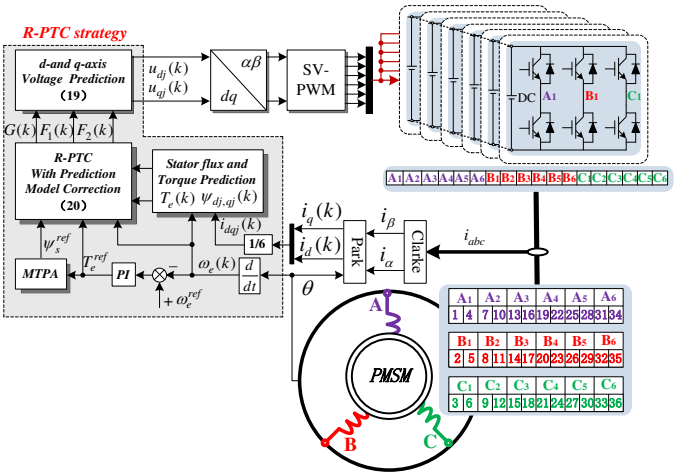

*Fig. 5. Structural diagram of the 6*3-phase PMSM drive system with R-PTC strategy.*

V. SIMULATIONS

In order to demonstrate the effectiveness of the proposed R-PTC strategy, the proposed R-PTC method in one *6**3-phase SPMSM system are carried out in MATLAB/ Simulink. Some simulation results are performed in comparisons with conventional PTC. The main parameters of *6**3-phase SPMSM used in the simulation are given in Tables I. The weight factor of conventional PTC method is 5000. The proportion coefficient and integral coefficient in PI controller of speed control loop are 8000 and 0.5, respectively. In addition, the sampling frequency is 10 kHz; the proportional parameters of proposed R-PTC strategy are Q_1=1 and Q_2=Q_3=50 .

Table I: MAIN PARAMETERS OF *6**3-PHASE SPMSM

Parameters	Value
Stator phase resistance(R_o)	0.02Ω
Number of pole pairs (n_p)	4
Inductances(L_o)	3.572mH
Flux linkage of PM (Ψ_{ro})	0.892Wb
Rotational inertia (J)	100kg.m^2

A. Control Performance Comparison between Conventional PTC and Proposed R-PTC without Parameter Mismatch

Comparative simulation results of conventional PTC and proposed R-PTC without parameter mismatch are depicted in Figs. 6-9. The load torque suddenly increases from 800 to 1600 N.m at 1s, and it suddenly decreases to 800 N.m at 1.4s. The speed reference is set as 100rad/s at 0s. The simulation results of α-β stator flux linkage and three-dimensional rotor flux trajectories are shown in Figs. 6 and 7, respectively. The stator flux linkage ripples are respectively ±0.02Wb and ±0.04Wb for proposed R-PTC and the conventional PTC, as presented in Figs. 6(a) and 6(b). The error between the predicted α-β flux linkage value and its reference value is very small, which are shown clearly in Figs. 7(a) and 7(b). Figs. 8 depict the torque ripple with the two methods under normal conditions. The peak-to-peak torque ripple of proposed R-PTC and the conventional PTC are basically the same, both of which are about ±200N.m. Figs. 9 present the frequency spectra of the stator current i_a at 1600N.m. The total harmonics distortion (THD) of stator current is 0.98% for the proposed R-PTC and 2.53% for conventional PTC. Through the simulation results analysis, it can be known that both the conventional PTC and proposed R-PTC have good control performance in this case.

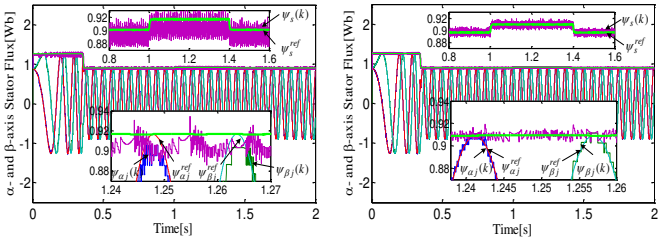

(a) Conventional PTC (b) Proposed R-PTC

Fig.6. Simulation results of the α-β stator flux linkage.

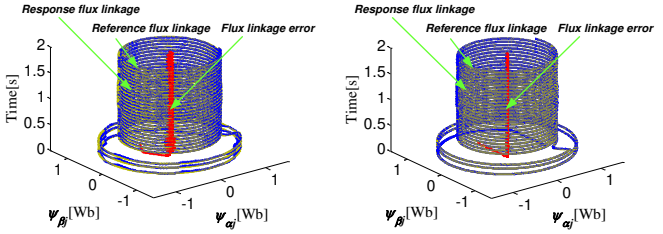

(a) Conventional PTC (b) Proposed R-PTC

Fig.7. Simulation results of three-dimensional rotor flux trajectories.

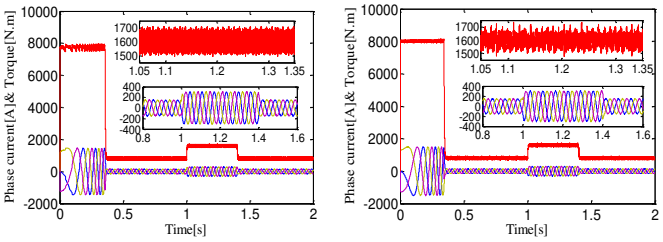

(a) Conventional PTC (b) Proposed R-PTC

Fig.8. Simulation results of the phase current and torque.

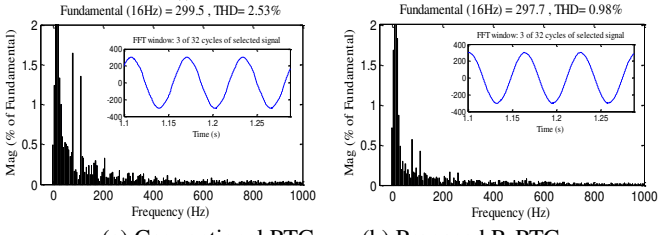

(a) Conventional PTC (b) Proposed R-PTC

Fig.9. The frequency spectra of stator current i_a at 1600N.m.

B. Control Performance Comparison between Conventional PTC and Proposed R-PTC under Flux Parameter Mismatch ($\Delta\psi_r = -50\%\psi_{ro}$)

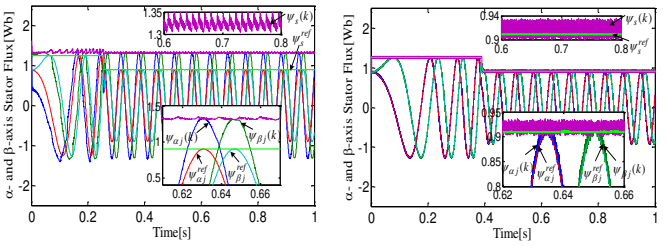

(a) Conventional PTC (b) Proposed R-PTC

Fig.10. Simulation results of the α-β stator flux linkage.

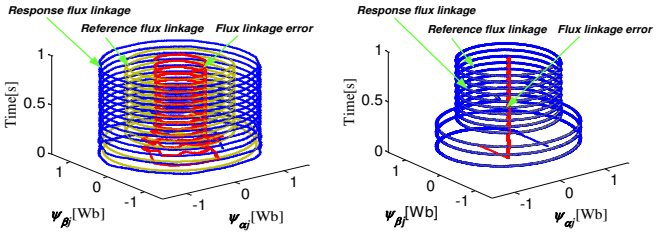

(a) Conventional PTC (b) Proposed R-PTC

Fig.11. Simulation results of three-dimensional rotor flux trajectories.

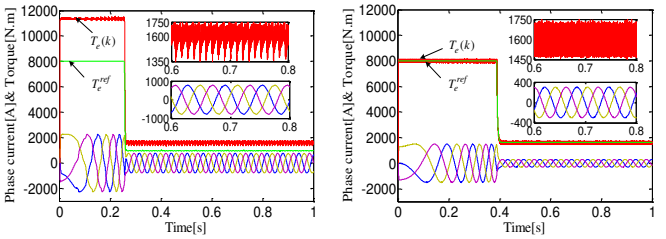

(a) Conventional PTC (b) Proposed R-PTC

Fig.12. Simulation results of the phase current and torque.

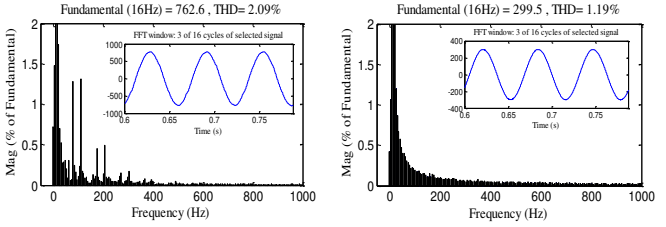

(a) Conventional PTC (b) Proposed R-PTC

Fig.13.The frequency spectra of stator current i_a at 1600N.m.

Comparative simulation results of conventional PTC and proposed R-PTC under flux parameter mismatch are shown in Figs. 10-13. At 0s, the load torque and speed reference are set as 1600 N.m and 100rad/s, respectively. From Figs. 10(a) and 11(a), it can be seen that there is a large static error between the predicted α-β stator flux value and the reference value, and the stator flux error is as high as ±0.43Wb. The stator flux error of the proposed R-PTC algorithm is only ±0.01Wb, which is significantly lower than that of the conventional PTC algorithm, as shown in Figs. 10(b) and 11(b). According to Figs. 10 and 11, it can be known that the flux parameter mismatch has a great influence on stator flux prediction and control in the conventional PTC algorithm. Figs. 12 show the torque ripple with the two methods under flux parameter mismatch. As it is seen, the peak-to-peak torque ripple is about ±400N.m for conventional PTC algorithm, and it decreases to ±300N.m for the proposed R-PTC algorithm in this case. Furthermore, compared with the conventional PTC algorithm, the predicted torque of the proposed R-PTC algorithm can accurately track the reference value. The reason is that the proposed R-PTC algorithm can effectively eliminate the influence of flux parameter mismatch by adjusting proportional parameters. It is seen from Fig. 13 that the THD of the proposed R-PTC and conventional PTC are 1.19% and 2.09%, respectively. Note that the fundamental value of the proposed R-PTC is 299.5, while that of the conventional PTC is 762.6. The reason for this phenomenon is that the proposed R-PTC can maintain the fundamental value unchanged by adjusting the proportional parameters. However, the stator current of the conventional PTC method should be large enough to keep the torque constant under flux parameter mismatch.

C. Control Performance Comparison between Conventional PTC and Proposed R-PTC under Inductance Parameter Mismatch ($\Delta L = -50\% L_o$)

Comparative simulation results of conventional PTC and proposed R-PTC under inductance parameter mismatch are shown in Figs. 14-17. At 0s, the load torque and speed reference step from 0 to 1600 N.m and 100 rad/s, respectively.

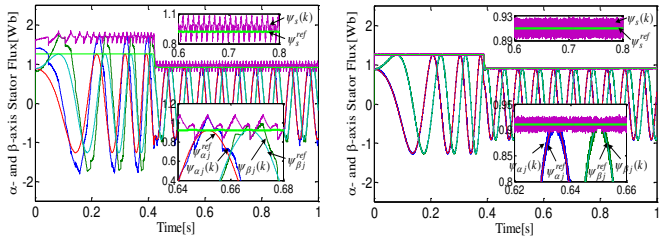

(a) Conventional PTC (b) Proposed R-PTC

Fig.14. Simulation results of the α-β stator flux linkage.

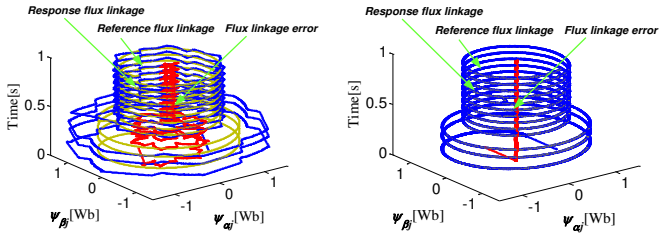

(a) Conventional PTC (b) Proposed R-PTC

Fig.15. Simulation results of three-dimensional rotor flux trajectories.

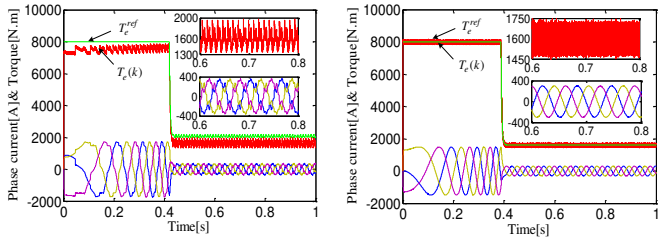

(a) Conventional PTC (b) Proposed R-PTC

Fig.16. Simulation results of the phase current and torque.

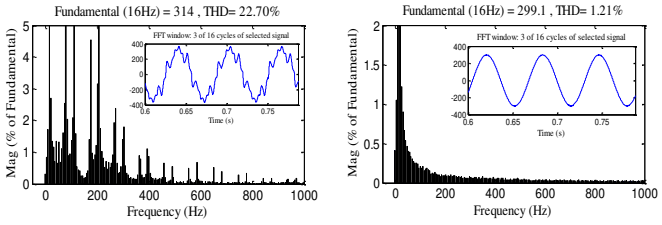

(a) Conventional PTC (b) Proposed R-PTC

Fig.17. The frequency spectra of stator current i_a at 1600N.m.

Figs. 14 and15 show the simulation results of α-β stator flux linkage and three-dimensional rotor flux trajectories under inductance parameter mismatch. From Figs. 14 and15, it can be seen that both the proposed R-PTC method and the conventional PTC method can accurately track the α-β stator flux linkage reference. However, the stator flux ripple of the conventional PTC method is as high as ±0.3Wb. The stator flux ripple has decreased to ±0.04Wb for the proposed R-PTC method, as shown in Figs. 14(a) and 14(b). The reason of the large stator flux ripple is that the inductance parameter mismatch will lead to the divergence of conventional PTC. Figs. 16 and17 depict the torque ripple and stator current frequency spectra under inductance parameter mismatch. Compared to the conventional PTC, the peak-to-peak torque ripple of proposed R-PTC method decreases from ±700 to ±300N.m, with a reduction of 57.1%, as presented in Fig. 16(b). From Fig.17, the THD of the conventional PTC under inductance parameter mismatch is 22.70%, whereas it is decreased to 1.21% by using the proposed R-PTC method. The reason for the large torque ripple and THD is that conventional PTC method is sensitive to inductance parameters. While in the proposed R-PTC method, the stator flux ripple, torque ripple and THD are drastically decreased for the reason that it is able to against inductance parameter mismatch.

*D. Control performance of the N*3-phase PMSM (N=3) under flux parameter mismatch.*

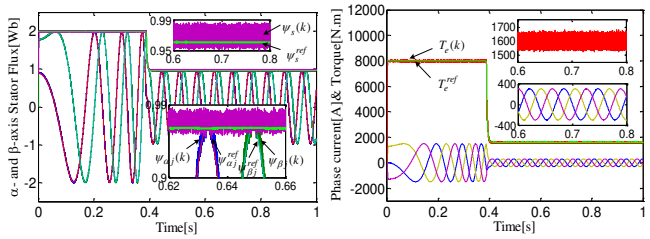

(a) The α-β stator flux linkage (b) The phase current and torque

*Fig.18. Simulation results of the 3*3-phase PMSM under flux parameter mismatch.*

The simulation results of the *3**3-phase PMSM under flux parameter mismatch are shown in Fig. 18. When the proposed R-PTC method is used to control the 3*3-phase PMSM, the α-β stator flux linkage response value can also accurately track the reference value, and the tracking error is only 0.02Wb, as presented in Figs. 18(a). From Figs. 18(b), it is known that the torque ripple of the *3**3-phase PMSM is less than ±200N.m by using the proposed R-PTC method. Through the simulation results analysis, it can be found that the proposed R-PTC method is immune to the parameter *N*. This type of motor can achieve the excellent control performance by adopting the proposed R-PTC method.

*E. Control performance of the N*3-phase PMSM under different proportion parameters mismatch ($\Delta L=-30\%L_o$)*

Simulation results of the *N**3-phase PMSM under different proportion parameters mismatch are shown in Fig. 19. The same controller parameters (i.e., Q1=1, Q2=Q3=50) is used to control the *N**3-phase PMSM with different proportion inductance parameter mismatch. From Fig. 19(a), it can be seen that the α-β stator flux linkage static error is essentially zero in the steady state. The torque response value can accurately track the reference value, and the peak-to-peak torque ripple is also ±300N.m, which are shown clearly in Fig. 19(b). Through the results analysis, it can be known that the *N**3-phase PMSM with different proportion parameter mismatch can also achieve excellent control performance by using the same controller parameters.

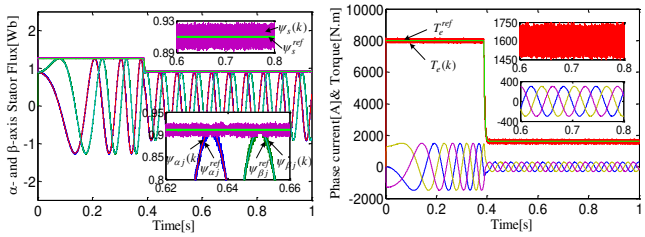

(a) The α-β stator flux linkage (b) The phase current and torque

Fig.19. Simulation results of the proposed R-PTC method under different proportion parameter mismatch.

VI. EXPERIMENTAL VERIFICATION

To demonstrate the effectiveness of the proposed R-PTC method, the control hardware-in-the-loop[26, 35] experiments of the *6**3-phase SPMSM drive system is carried out, as shown in Figs. 21-24. The RT-Lab hardware-in-the-loop simulation (HILS) platform is shown in Fig. 20. The RT-Lab HILS platform is composed of the OP5600 simulation motor, DSP controller, and *6**3-phase PMSM system model as software component. The HILS of *6**3-phase PMSM drive system can be simulated by establishing the compiled code of *6**3-phase PMSM and using the inverter model in OP5600. The proposed R-PTC method is performed on the platform of the TMS320F2812 processor. The system parameters are consistent with simulation parameters.

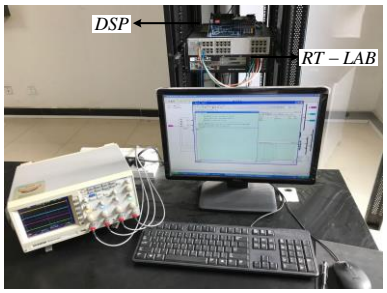

Fig.20 hardware-in-the loop simulation platform.

Fig. 21 shows a comparison of the proposed R-PTC and the conventional PTC without parameter mismatch. Similar to the simulation, the load torque is given a step reference in the steady-state process. Fig. 21(a) shows the experimental results of the phase current, torque and stator flux when the conventional PTC is adopted. The torque ripple and stator flux ripple are about 0.6 and 0.55 (p.u.), respectively. Fig. 21(b) shows the experimental results of the phase current, torque and stator flux with the proposed R-PTC. The torque ripple and stator flux ripple are about 0.55 and 0.5 (p.u.), respectively. It can be seen that the proposed R-PTC method has the same superiority as the conventional PTC method in this case.

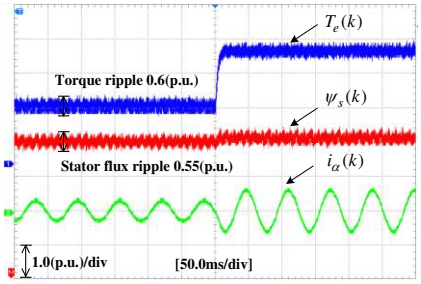

(a) Conventional PTC

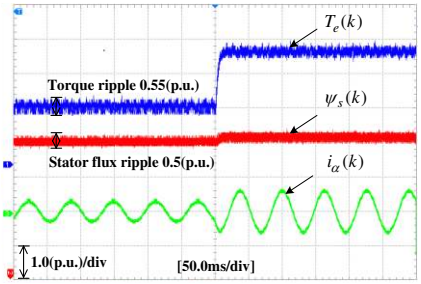

(b) Proposed R-PTC

Fig.21. Experimental results of the phase current, torque and stator flux without parameter mismatch.

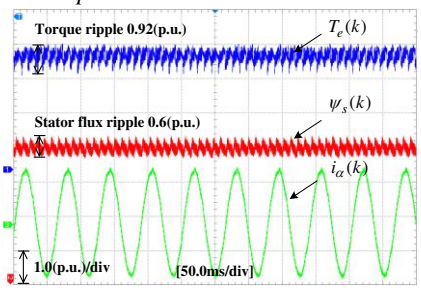

(a) Conventional PTC

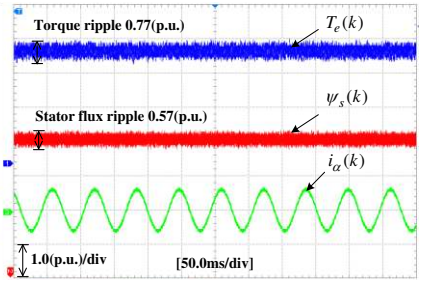

(b) Proposed R-PTC

Fig.22. Experimental results of the phase current, torque and stator flux under flux parameter mismatch.

Fig. 22 shows a comparison of the proposed R-PTC and the conventional PTC under flux parameter mismatch. From Fig. 22(a), the torque ripple and stator flux ripple of conventional PTC are about 0.92 and 0.6 (p.u.), respectively. By comparing Fig. 22(a) and (b), the stator flux ripple of proposed R-PTC is basically unchanged, about 0.57 (p.u.). However, the torque ripple of proposed R-PTC is significantly reduced by up to 16%, from 0.92 to 0.77 (p.u.). According to the quantitative comparison, it is obvious that the torque ripple can be effectively suppressed by adopting the proposed R-PTC method. Note that the stator current of the conventional PTC method is obviously larger than that of the proposed R-PTC method. The reason is that the stator current is large enough to keep the torque constant in the absence of compensation link.

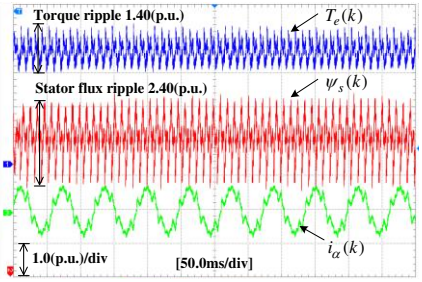

(a) Conventional PTC

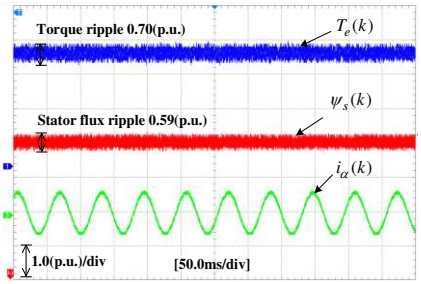

(b) Proposed R-PTC

Fig.23. Experimental results of the phase current, torque and stator flux under inductance parameter mismatch.

Fig. 23 shows a comparison of the proposed R-PTC and the conventional PTC under inductance parameter mismatch. From Fig. 23(a), it can be seen that inductance parameter mismatch have a huge influence on the control performance of the conventional PTC. Large ripples exist in the stator flux and torque when the predictive controller parameters do not match the actual motor parameters. Furthermore, the stator current will be distorted obviously. When the proposed R-PTC method is adopted, the torque ripple is significantly reduced by up to 50%, from 1.40 to 0.70 (p.u.), and the stator flux ripple is significantly decreased by up to 75%, from 2.40 to 0.59 (p.u.), as shown in Fig. 23(b). From Fig. 23, it is known that proposed R-PTC method can obtain satisfactory control performance under inductance parameter mismatch, which verify the feasibility and superiority of the proposed methods compared with the conventional PTC method.

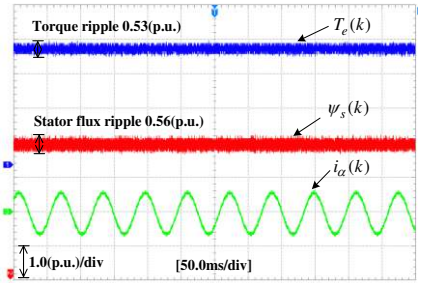

*Fig.24. Experimental results of the N*3-phase PMSM (N=3) under flux parameter mismatch.*

Fig. 24 shows the experimental results of the *3**3-phase PMSM by using the proposed R-PTC. When the proposed R-PTC method is used to control the *3**3-phase PMSM, the torque ripple and stator flux ripple of *3**3-phase PMSM with flux parameter mismatch are about 0.53 and 0.56 (p.u.), respectively. By comparing the experimental results of Fig. 24 and Fig. 22 (b) show that the control performance of *3**3-phase PMSM is as good as that of *6**3-phase PMSM when the proposed R-PTC method is adopted. Through the experimental results analysis, it is known that the proposed R-PTC method is not affected by the number (*N*) of motor units.

VII. Conclusion

In this paper, a novel R-PTC technique of *N*-segment three-phase PMSM drives is proposed for high power traction applications. The proposed R-PTC method for *N*-segment three-phase PMSM has been proved to give excellent control performance, effectively controlling both the electromagnetic torque and the stator flux. The stator flux and torque error-based cost function is replaced by the motor model-based voltage vector equation in R-PTC to avoid the adjustment of weighting factor. Furthermore, the proposed R-PTC method utilizes the proportional controller to adjust the control voltage vector, so as to eliminate the influence of model parameter mismatch. Compared to the conventional PTC, the proposed R-PTC method can significantly improve the predictive accuracy of the stator flux and torque, and decrease the tracking errors under parameters mismatch. The simulation and experimental results obtained demonstrate the effectiveness of the proposed R-PTC method, which can achieve the merits of lower stator current THD, less torque ripple and excellent dynamic performance under parameters mismatch.

References

[1] S. Morimoto, Y. Tong, Y. Takeda, and T. Hirasa, "Loss minimization control of permanent magnet synchronous motor drives," *IEEE Trans. Ind. Electron*., vol. 41, no. 5, pp. 511-517, Oct. 1994.

[2] T. Jahns, G. Kliman, and T. Neumann, "Interior permanent-magnet synchronous motors for adjustable-speed drives," *IEEE Trans. Ind. Applicat*., vol. 22, no. 4, pp. 738-747, Jul./Aug. 1986.

[3] Z. Chen, M. Tomita, S. Doki, and S. Okuma, "An extended electromotive force model for sensorless control of interior permanent-magnet synchronous motors," *IEEE Trans. Ind. Electron*., vol. 50, no. 2, pp. 288-295, Apr. 2003.

[4] S. Morimoto, Y. Takeda, and T. Hirasa, "Current phase control methods for permanent magnet synchronous motors," *IEEE Trans. Power Electron*., vol. 5, no. 2, pp. 133-139, Apr. 1990.

[5] E. Levi, "Multiphase electric machines for variable-speed applications," *IEEE Trans. Ind. Electron*., vol. 55, no. 5, pp. 1893-1909, May. 2008.

[6] Y. Hu, Z. Zhu, and M. Odavic, "Torque capability enhancement of dual three-phase PMSM drive with fifth and seventh current harmonics injection," *IEEE Trans. Ind. Electron*., vol. 53, no. 5, pp. 4526-4535, Sep./Oct. 2017.

[7] E. Levi, M. Jones, S. Vukosavic, and H. Toliyat, "A novel concept of a multiphase, multimotor vector controlled drive system supplied from a single voltage source inverter," *IEEE Trans. Power Electron*., vol. 19, no. 2, pp. 320-225, Mar. 2004.

[8] L. Shao, W. Hua, N. Dai, M. Tong, and M. Cheng, "Mathematical modeling of a 12-phase flux-switching permanent-magnet machine for wind power generation," *IEEE Trans. Ind. Electron*., vol. 63, no. 1, pp. 504-516, Jan. 2016.

[9] M. Onsal, Y. Demir, and M. Aydin, "A new nine-phase permanent magnet synchronous motor with consequent pole rotor for high-power traction applications," *IEEE Trans. Magn.*, vol. 53, no. 11, pp. 1-6, Nov. 2009.

[10] H. Che, E. Levi, M. Jones, W. Hew, and N. Rahim, "Current control methods for an asymmetrical six-phase induction motor drive," *IEEE Trans. Power Electron.*, vol. 29, no. 1, pp. 407-417, Jan. 2014.

[11] X. Wang, Z. Wang, Z. Xu, "A hybrid direct torque control scheme for dual three-phase PMSM drives with improved operation performance," *IEEE Trans. Power Electron.*, vol. 34, no. 2, pp. 1622-1634, Feb. 2018.

[12] J. Karttunen, S. Kallio, P. Peltoniemi, P. Silventoinen, and O. Pyrhönen, "Decoupled vector control scheme for dual three-phase permanent magnet synchronous machines," *IEEE Trans. Ind. Electron*., vol. 61, no. 5, pp. 2185-2196, May. 2014.

[13] Y. Demir, and M. Aydin, "A novel asymmetric and unconventional stator winding configuration and placement for a dual three-phase surface PM motor," *IEEE Trans. Magn.*, vol. 53, no. 11, pp. 1-5, Nov. 2017.

[14] X. Han, D. Jiang, T. Zou, R. Qu, and K. Yang, "Two-Segment Three-Phase PMSM Drive With Carrier Phase-Shift PWM for Torque Ripple and Vibration Reduction," *IEEE Trans. Power Electron.*, vol. 34, no. 1, pp. 588-599, Jan. 2019.

[15] X. Han, D. Jiang, T. Zou, R. Qu, and K. Yang, "Two-segment three-phase PMSM drive with carrier phase-shift PWM," in *IEEE APEC*, Mar. 2018, pp. 848-854.

[16] S. Bhattacharya, D. Mascarella, G. Joós, J. Cyr, and J. Xu, "A dual three-level T-NPC inverter for high-power traction applications," *IEEE J. Emerg. Sel. Topics Power Electron.*, vol. 4, no. 2, pp. 668-678, Jun. 2016.

[17] S. Bhattacharya, D. Mascarella, G. Joós, " Interleaved PWM control for neutral point balancing in dual 3-level traction drives," in *Proc. IEEE ECCE*, USA, Sept. 2014, pp. 1715-1721.

[18] S. Li, and Z. Liu, "Adaptive speed control for permanent magnet synchronous motor system with variations of load inertia," *IEEE Trans. Ind. Electron*., vol. 56, no. 8, pp. 3050-3059, Aug. 2009.

[19] X. Zhang, Y. He, "Direct Voltage-Selection Based Model Predictive Direct Speed Control for PMSM Drives without Weighting Factor," *IEEE Trans. Power Electron*., vol. 34, no. 8, pp. 7838-7851, Jan. 2018.

[20] C. Rojas, J. Rodriguez, F. Villarroel, J. Espinoza, C. Silva, and M. Trincado, "Predictive torque and flux control without weighting factors," *IEEE Trans. Ind. Electron*., vol. 60, no. 2, pp. 681-690, Feb. 2013.

[21] S. Davari, D. Khaburi, R. Kennel, "An improved FCS–MPC algorithm for an induction motor with an imposed optimized weighting factor," *IEEE Trans. Power Electron.*, vol. 27, no. 3, pp. 1540-1551, Mar. 2012.

[22] X. Zhang, B. Hou, "Double vectors model predictive torque control without weighting factor based on voltage tracking error," *IEEE Trans. Power Electron.*, vol. 33, no. 3, pp. 2368-2380, Mar. 2018.

[23] J. Rodriguez, R. M. Kennel, J. R. Espinoza, M. Trincado, C. A. Silva, and C. A. Rojas, "High-performance control strategies for

electrical drives: An experimental assessment," *IEEE Trans. Ind. Electron*., vol. 59, no. 2, pp. 812-820, Feb. 2012.

[24] X. Zhang, Zhang. Liang, and Y. Zhang, "Model predictive current control for PMSM drives with parameter robustness improvement," *IEEE Trans. Power Electron*., vol. 34, no. 2, pp. 1645-1657, Feb. 2018.

[25] S. Huang, G. Wu, F. Rong, C. Zhang, S. Huang, and Q. Wu, "Novel Predictive Stator Flux Control Techniques for PMSM drives," *IEEE Trans. Power Electron.*, vol. 34, no. 9, pp. 8916-8929, Sep. 2018.

[26] C. Zhang, G. Wu, F. Rong, and J. Feng, "Robust fault-tolerant predictive current control for permanent magnet synchronous motors considering demagnetization fault," *IEEE Trans. Ind. Electron*., vol. 65, no. 7, pp. 5324-5534, Jul. 2017.

[27] X. Zhang, B. Hou, and Y. Mei, "Deadbeat predictive current control of permanent-magnet synchronous motors with stator current and disturbance observer," *IEEE Trans. Power Electron*., vol. 32, no. 5, pp. 3818-3834, May. 2017.

[28] M. Yang, X. Lang, J. Long, and D. Xu, "A flux immunity robust predictive current control with incremental model and extended state observer for PMSM drive," *IEEE Trans. Power Electron*., vol. 32, no. 12, pp. 9267-9279, Dec. 2017.

[29] S. A. Davari, D. Khaburi, F. Wang, et al, "Using full order and reduced order observers for robust sensorless predictive torque control of induction motors," *IEEE Trans. Power Electron*., vol. 27, no. 7, pp. 3424-3433, Vol. 2012.

[30] F. Wang, S. A. Davari, Z. Chen, et al, "Finite control set model predictive torque control of induction machine with a robust adaptive observer," *IEEE Trans. Ind. Electron*., vol. 64, no. 4, pp. 2631-2641, Apr. 2017.

[31] J. Wang, F. Wang, Z. Zhang, et al, "Design and implementation of disturbance compensation-based enhanced robust finite control set predictive torque control for induction motor systems," *IEEE Trans. Ind. Informat*., vol. 13, no. 5, pp. 2645-2656, Oct. 2017.

[32] M. Siami, D. A. Khaburi, J. Rodriguez, "Torque ripple reduction of predictive torque control for PMSM drives with parameter mismatch," *IEEE Trans. Power Electron.*, vol. 32, no. 9, pp. 7160-7168, Sep. 2017.

[33] J.-F. Stumper, S. Kuehl, and R. Kennel, "Predictive torque control for AC drives: Improvement of parametric robustness using two-degree-offreedom control," in Proc. *IEEE Energy Convers. Congr. Expo.,* 2013, pp. 1170–1175.

[34] E. Jung, H. Yoo, S. Sul, H. Choi, and Y. Choi, " A nine-phase permanent-magnet motor drive system for an ultrahigh-speed elevator," *IEEE Trans. Ind. Applicat*., vol. 48, no. 3, pp. 987-995, May./Jun. 2012.

[35] Z. Shuai, W. Huang, Z. Shen, "Characteristics and restraining method of fast transient inrush fault currents in synchronverters," *IEEE Trans. Ind. Electron*., vol. 64, no. 9, pp. 5324-5534, Sep. 2017.

Gongping Wu was born in Jiangxi, China. He studied at Tongji University, Shanghai, China, from September 2011 to September 2013. He received the B.S. degree from Jinggangshan University, Jiangxi, China, in 2014, and the M.S. degree from the Hunan University of Technology, Hunan, China, in 2017, both in electrical engineering and automation. Since September 2017, he has been working toward the Ph.D. degree at the College of Electrical and Information Engineering, HunanUniversity, Changsha, China. During 2019–2021, he was a visiting student in the Department of Electrical Engineering, Technical University of Denmark, Kgs. Lyngby, Denmark.

His current research interests include permanent magnet synchronous motor servosystems, predictive current control, and wind energy conversion system.

Sheng Huang was born in Hunan, China. He received the M.S. and Ph.D. degree both in College of Electrical and Information Engineering, Hunan University, Changsha, China, in 2012 and 2016, respectively. He is currently a Postdoc with the Center for Electric Power and Energy, Technical University of Denmark.

His research interests include renewable energy generation, modeling and integration study of wind power, control of energy storage system, and voltage control.

Qiuwei Wu (M'08-SM'15) obtained the PhD degree in Power System Engineering from Nanyang Technological University, Singapore, in 2009.

He was a senior R&D engineer with VESTAS Technology R&D Singapore Pte Ltd from Mar. 2008 to Oct. 2009. He has been working at Department of Electrical Engineering, Technical University of Denmark (DTU) since Nov. 2009 (PostDoc Nov. 2009-Oct. 2010, Assistant Professor Nov. 2010-Aug. 2013, Associate Professor since Sept. 2013). He was a visiting scholar at Department of Industrial Engineering & Operations Research (IEOR), University of California, Berkeley, from Feb. 2012 to May 2012 funded by Danish Agency for Science, Technology and Innovation (DASTI), Denmark. He was a visiting professor named by Y. Xue, an Academician of Chinese Academy of Engineering, at Shandong University, China, from Nov. 2015 to Oct. 2017. He was a visiting scholar at the Harvard China Project, School of Engineering and Applied Sciences, Harvard University from Nov. 2017 – Oct. 2018.

His research interests are operation and control of power systems with high penetration of renewables, including wind power modelling and control, active distribution networks, and operation of integrated energy systems. He is an Editor of IEEE Transactions on Smart Grid and IEEE Power Engineering Letters. He is also an Associate Editor of International Journal of Electrical Power and Energy Systems, and Journal of Modern Power Systems and Clean Energy. He is a subject editor for IET Generation, Transmission & Distribution, and IET Renewable Power Generation.

Fei Rong (M'15) was born in Hubei, China, in 1978. He received the B.S. and M.S. degrees in control science and engineering from Central South University, Changsha, China, in 2000 and 2003, respectively. He also received Ph.D. degree in electrical engineering from Hunan University, Changsha, China, in 2008. He was a lecture from 2008 to 2010, and since 2011, has been an Associate Professor of electrical engineering in the College of Electrical and information engineering, Hunan University. In 2015, he became a member of the IEEE.

His interests include distributed power generation, reactive power compensation and active power filters.

Changfan Zhang was born in Hubei, China, in 1960. He received the M.S. degree in electronics engineering from Southwest Jiaotong University, Chengdu, China, in 1989, and Ph.D. degree in control theory and engineering from Hunan University, Changsha, China, in 2001. He was a Post-Doctoral Fellow at Central South University, Changsha, China, from October 2001 to October 2003, and a Visiting Research Fellow at University of Waterloo, Waterloo, Canada, from May 2007 to April 2008. Since February 1982, he has been with the College of Electrical and Information Engineering, Hunan University of Technology, Zhuzhou, China, and has been a Professor there since 2001.

His research interests include fault diagnosis on electrical machines and industrial process control.

Wu Liao was born in Hunan, China. He received the B.S. and Ph.D. degree both in College of Electrical and Information Engineering, Hunan University, Changsha, China, in 2010 and 2016, respectively. He was with CRRC Zhuzhou Institute Co., Ltd., Zhuzhou, China, as a converter software designer and researcher between 2016 and 2019. He is currently with Hunan University as a Postdoctoral Researcher at the Department of Electrical Engineering.

His research interests include wind power generation, modular multilevel converters, and high power motor drives.